INSTITUTE OF PHYSICS PUBLISHING JOURNAL OF PHYSICS: CONDENSED MATTER

J. Phys.: Condens. Matter **16** (2004) 4025–4032 PII: S0953-8984(04)75744-6

Intermediate valence behaviour in the new Kondo lattice compound $Yb_3Ni_5Al_{19}$

E D Bauer[1], S Bobev[1], J D Thompson[1], M F Hundley[1], J L Sarrao[1], A Lobos[2] and A A Aligia[2]

[1] Los Alamos National Laboratory, Los Alamos, NM 87545, USA
[2] Centro Atómico Bariloche and Instituto Balseiro, Comisión Nacional de Energía Atómica, 8400 SC de Bariloche, Argentina

Received 3 February 2004
Published 28 May 2004
Online at stacks.iop.org/JPhysCM/16/4025
DOI: 10.1088/0953-8984/16/23/019

Abstract

The physical properties of single crystals of the Kondo lattice material $Yb_3Ni_5Al_{19}$ have been investigated by means of magnetic susceptibility, specific heat, and electrical resistivity measurements. Single-crystal x-ray diffraction measurements indicate that $Yb_3Ni_5Al_{19}$ adopts the $Gd_3Ni_5Al_{19}$ orthorhombic crystal structure. This compound exhibits intermediate valence behaviour with a characteristic energy scale $T_K \sim 500$ K. Calculations of $\chi(T)$ based on the Anderson impurity model within the non-crossing approximation including crystalline electric field effects are also presented.

1. Introduction

In the past two decades, a large amount of effort has been devoted to the investigation of Ce-based Kondo lattice (KL) compounds due the to variety of novel strongly correlated electron behaviour observed in these systems such as heavy fermion behaviour, non-Fermi liquid behaviour, the coexistence of superconductivity and magnetism, and pressure induced superconductivity. The nature of the ground state in KL materials depends on a sensitive balance between competing Kondo and RKKY interactions, with characteristic energy scales $T_K \sim \exp(-1/N(E_F)|\mathcal{J}|)$ and $T_{RKKY} \sim \mathcal{J}^2 N(E_F)$, respectively, where $\mathcal{J}$ is the hybridization strength between the f electron and conduction electron states and $N(E_F)$ in the density of states at the Fermi level [1]. For $T_K \ll T_{RKKY}$, the RKKY interaction dominates leading to a magnetically ordered ground state; heavy fermion behaviour is expected for $T_K \sim T_{RKKY}$, and intermediate valence behaviour for $T_K \gg T_{RKKY}$. This situation is also expected to be realized in Yb-based KL compounds, which can be considered the $4f^{13}$ hole analogue to the Ce $4f^1$ electron configuration; however, comparatively little research has been carried out on such Yb materials as synthesis of Yb intermetallic compounds is difficult due to the high vapour pressure of Yb.

An initial attempt to synthesize single crystals of Yb–T–Ga (T = Co, Rh, Ir) in order to investigate the Kondo lattice behaviour in this ternary system yielded the intermediate valence materials $Yb_2Rh_3Ga_9$ and $Yb_2Ir_3Ga_9$ [2]. These two compounds belong to the family $R_2T_3X_9$ (R = Ce, Yb, U; T = Co, Rh, Ir; X = Al, Ga) that crystallize in the orthorhombic $Y_2Co_3Ga_9$-type structure and have been extensively investigated in recent years [3–7]. Our recent efforts to explore the Yb–T–Al ternary system have yielded a new Kondo lattice compound $Yb_3Ni_5Al_{19}$ which crystallizes in the orthorhombic $Gd_3Ni_5Al_{19}$ structure type [8]. In this paper, we report the physical properties of $Yb_3Ni_5Al_{19}$ including magnetic susceptibility χ, specific heat C, and electrical resistivity ρ measurements, which reveal intermediate valence behaviour with a characteristic energy scale $T_K \sim 500$ K. Calculations of $\chi(T)$ based on the Anderson impurity model within the non-crossing approximation (NCA) including crystalline electric field (CEF) effects are presented.

2. Experimental details

Single crystals of $Yb_3Ni_5Al_{19}$ were grown in Al flux. The elements were placed in an alumina crucible in the ratio Yb:Ni:Al = 1:1:20 and sealed in a quartz tube under vacuum. The materials were heated to 1100 °C and kept there for 2 h; this was followed by slow cooling to 600 °C at a rate 10 °C h^{-1} at which point excess Al was removed in a centrifuge. The single crystals were long needles with typical dimensions of $0.5 \times 0.5 \times 10$ mm^3.

Single-crystal x-ray diffraction data were collected at $T = 90(2)$ K on a Bruker SMART 1000 CCD diffractometer. A hemisphere of data was collected for a plate-like crystal of dimensions $0.12 \times 0.10 \times 0.04$ mm^3 using Mo Kα radiation ($2\theta_{max} = 63°$). The data were corrected for Lorentz and polarization effects and merged in Laue symmetry *mmm* (3749 total reflections, 1411 unique reflections, $R_{int} = 4.71\%$) using the SMART[3] and SAINT[4] software. A semi-empirical absorption correction was applied with the aid of the SADABS software package[5]. The structure was solved by direct methods and subsequently refined with the use of the SHELXTL V5.10 package[6]. The crystal structure was determined to be of the orthorhombic $Gd_3Ni_5Al_{19}$ type (space group *Cmcm*) [8]. Further details of the data collection and structure refinement parameters of $Yb_3Ni_5Al_{19}$ are given in table 1 and footnote 7[7].

The magnetic susceptibility measurements were performed in a SQUID magnetometer (Quantum Design) from 2 to 350 K in a magnetic field $H = 1$ and 50 kOe on a collection of single crystals. The specific heat was measured from 2 to 300 K using a thermal relaxation method. The electrical resistivity measurements were performed from 2 to 300 K using a Linear Research LR-700 ac-resistance bridge with an excitation current of 1 mA along one of the principal directions.

3. Results

3.1. Single-crystal x-ray diffraction

A schematic representation of the orthorhombic structure of $Yb_3Ni_5Al_{19}$ is shown in figure 1. This compound represents only the second example of a ternary R–Ni–Al intermetallic phase

[3] SMART NT Version 5.05, Bruker Analytical X-ray Systems, Inc., Madison, WI, 1998.
[4] SAINT NT Version 6.22, Bruker Analytical X-ray Systems, Inc., Madison, WI, 2001.
[5] SADABS NT Version 2.05, Bruker Analytical X-ray Systems, Inc., Madison, WI, 1998.
[6] SHELXTL Version 5.10, Bruker Analytical X-ray Systems, Inc., Madison, WI, 1997.
[7] Further details of the crystal structure investigation may be obtained from the Fachinformationszentrum Karlsruhe, 76344 Eggenstein-Leopoldshafen, Germany (fax: (+49) 7247-808-666; e-mail: crysdata@fiz-karlsruhe.de) with the depository number CSD-413702.

Table 1. Selected data collection and crystal structure refinement parameters for $Yb_3Ni_5Al_{19}$; $Gd_3Ni_5Al_{19}$ type; space group $Cmcm$ (No 63); range of scattering angle $3° < 2\theta < 63°$; Mo Kα radiation ($\lambda = 0.710\,73$ Å). The parentheses indicate the uncertainties in the last digit.

Parameter				
T (K)	90(2)			
Lattice parameter				
a (Å)	4.0635(4)			
b (Å)	15.901(1)			
c (Å)	26.983(2)			
Volume V (Å^3)	1743.5(3)			
Density ρ (g cm^{-3})	5.049			
No of f.u. per unit cell Z	4			
Unique reflections	1411			
Number of variables	86			
$R_1 = \frac{\sum \|\|F_0\|-\|F_c\|\|}{\sum \|F_0\|}$	3.24%			
$wR_2 = \sqrt{\frac{\sum w(F_0^2-F_c^2)^2}{\sum w(F_0^2)^2}}$, where $w = 1/(\sigma^2 F_0^2)$	5.74%			
GOF	1.07			
Atom parameters				
	x	y	z	U_{iso}[a] (Å^2)
Yb(1)	0	0.1089(1)	1/4	0.007(1)
Yb(2)	0	0.3337(1)	0.3647(1)	0.007(1)
Ni(1)	0	0.4350(1)	1/4	0.008(1)
Ni(2)	0	0.1591(1)	0.5420(1)	0.006(1)
Ni(3)	0	0.4463(1)	0.5850(1)	0.008(1)
Al(1)	0	0.0939(2)	0.0373(1)	0.009(1)
Al(2)	0	0.7221(2)	0.3062(1)	0.009(1)
Al(3)	0	0.0824(2)	0.7017(1)	0.009(1)
Al(4)	0	0.2903(2)	0.5895(1)	0.008(1)
Al(5)	0	0.2656(2)	0.4710(1)	0.009(1)
Al(6)	0	0.0380(2)	0.6015(1)	0.009(1)
Al(7)	0	0.1301(2)	0.1358(1)	0.009(1)
Al(8)	0	0.5674(2)	0.5317(1)	0.009(1)
Al(9)	0	0.5343(2)	0.3254(1)	0.010(1)
Al(10)	0	0.3032(3)	1/4	0.011(1)

[a] U_{iso} is defined as one third of the trace of the orthogonalized U_{ij} tensor.

(R = rare earth) with the $Gd_3Ni_5Al_{19}$ type of structure. The rather complicated $Yb_3Ni_5Al_{19}$ structure can be regarded as an intergrowth between the imaginary structures of $YbNiAl_4$ (with the orthorhombic $YNiAl_4$-type structure [9]) and that of $Yb_2Ni_4Al_{15}$ (monoclinic). This $Gd_3Ni_5Al_{19}$ structure is the simplest member ($m = 1$) of the family of compounds $R_{2+m}T_{4+m}Al_{15+4m}$, where m is the number of $RNiAl_4$-type units, in which the materials with m odd adopt an orthorhombic structure and even-m members adopt a monoclinic structure (i.e., $m = 2$, $Gd_4Ni_6Al_{23}$ [10]).

There are two crystallographically unique Yb sites, three unique Ni sites, and ten unique Al sites in the asymmetric unit cell of the $Yb_3Ni_5Al_{19}$ structure. Despite the apparent structural complexity, all atomic positions are well ordered and there is no evidence for occupational disorder as deduced from the well-defined atomic displacement parameters. As can be seen from figures 1(b) and (c), the two Yb sites, although crystallographically inequivalent, have

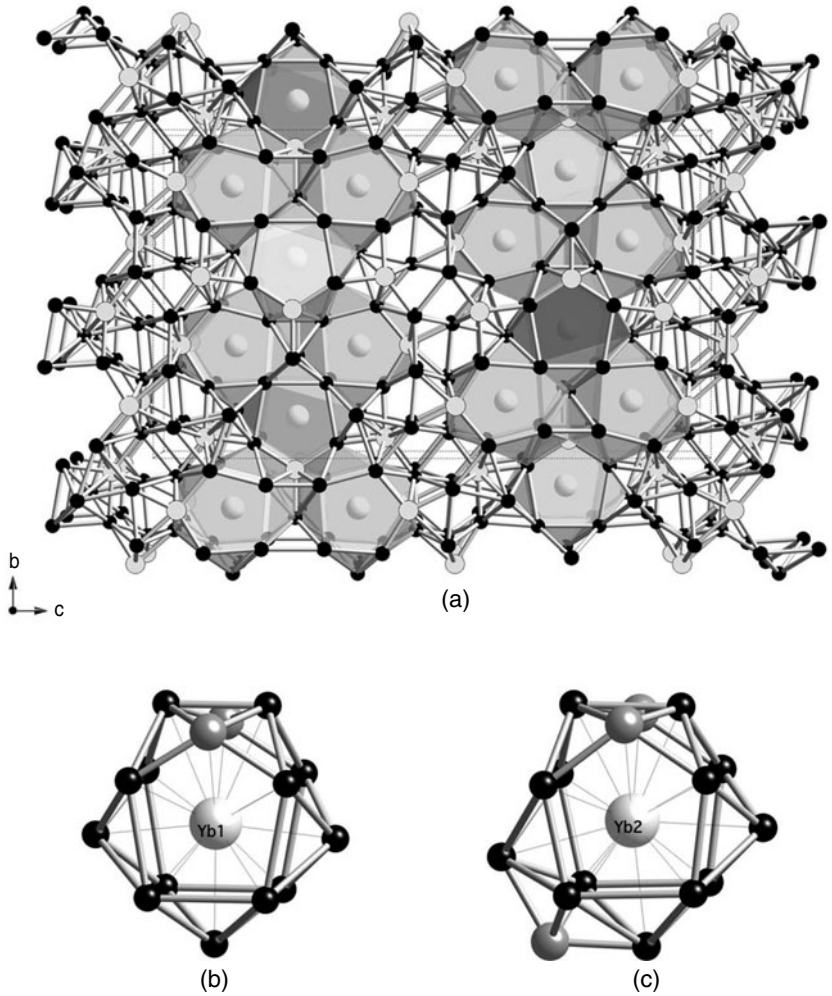

Figure 1. (a) The crystal structure of $Yb_3Ni_5Al_{19}$. Yb—large grey spheres, Ni—small grey spheres, Al atoms—small black spheres. The two crystallographically unique ytterbium atoms reside in channels running along the [100] direction and are highlighted as translucent polyhedra. (b) and (c) show the first coordination spheres of Yb(1) and Yb(2), respectively.

quite similar coordination environments. The Yb(1) site is situated in the centre of a 15-atom polyhedron comprised of 13 Al and 2 Ni(1) atoms. The corresponding Yb(1)–Al distances range from 3.089 to 3.310 Å, while the Yb(1)–Ni(1) distance is 3.206 Å. The Yb(2) site coordination polyhedron appears very similar, although it has 16 nearest neighbours (13 Al and 3 Ni atoms) and the Yb(2)-centred polyhedron is slightly distorted in comparison with the Yb(1)-centred one. A somewhat broader range of Yb(2)–Al distances is found, from 3.019 to 3.362 Å, compared to the Yb(1)–Al distances. Also, there are two shorter Yb(2)–Ni(2) bonds (3.237 Å), and one significantly longer Yb(2)–Ni(1) bond at 3.629 Å.

3.2. Magnetic susceptibility

The magnetic susceptibility $\chi \equiv M/H$ versus temperature T for $Yb_3Ni_5Al_{19}$ is shown in figure 2. A broad maximum is present in the $\chi(T)$ data at $T_{max} \sim 100$ K and is typical

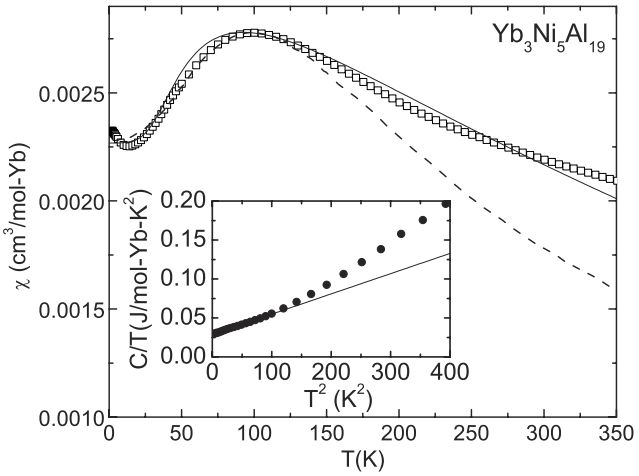

Figure 2. The magnetic susceptibility $\chi(T)$ of $Yb_3Ni_5Al_{19}$ measured in a magnetic field $H = 50$ kOe. The dashed curve is a single-impurity calculation from Rajan [13] and the solid curve is the Anderson impurity model calculation including intersite interactions and CEF effects discussed in the text. Inset: specific heat $C(T)$, plotted as C/T versus T^2. The solid line is a linear fit of the data.

of intermediate valence systems with a characteristic energy scale (Kondo temperature) $T_K \sim 500$ K. Above 250 K, the magnetic susceptibility can be fitted to a Curie–Weiss law (not shown) yielding an effective moment $\mu_{eff} = 4.25\ \mu_B$/mol Yb, somewhat smaller than the Yb^{3+} value of $\mu_{eff} = 4.54\ \mu_B$, and an unusually large Curie–Weiss temperature $\theta_{CW} = -731$ K suggesting the presence of strong antiferromagnetic correlations. While a magnetic field of 5.5 T suppresses the 'Curie tail' below 15 K by a factor of five or more, the overall magnitude of χ changes by at most ~0.3% from the value determined at $H = 0.1$ T (not shown), indicating that impurities of ferromagnetic Ni are not present [11]. There is no evidence for heterogeneous mixed valence behaviour, i.e., one of the two Yb sites having an Yb^{2+} configuration, as the effective moment (per mol Yb) is close to the Yb^{3+} free-ion value.

3.3. Heat capacity

The specific heat, plotted as $C(T)/T$ versus T^2, is displayed in the inset of figure 2. The low T $C(T)$ data were fitted by the expression $C/T = \gamma + \beta T^2$ in the range $2\ \text{K} \leqslant T \leqslant 10$ K yielding an electronic specific heat coefficient $\gamma = 29\ \text{mJ K}^{-2}\ (\text{mol Yb})^{-1}$ and $\beta = 0.26\ \text{mJ K}^{-4}\ (\text{mol Yb})^{-1}$ corresponding to a Debye temperature $\theta_D = 282$ K. In order to check whether the enhancements of χ and γ are due to itinerant electrons, the Wilson ratio $\mathcal{R}_W = (\pi^2 k_B^2/\mu_{eff})(\chi_0/\gamma_0)$ was calculated, where k_B is Boltzmann's constant, and χ_0 and γ_0 are the zero-temperature values of the magnetic susceptibility and electronic specific heat coefficient, respectively. Using the free-ion Yb^{3+} value $\mu_{eff} = 4.54\ \mu_B$, $\chi_0 = 0.002\,25\ \text{cm}^3/\text{mol Yb}$, and $\gamma_0 = 29\ \text{mJ K}^{-2}\ (\text{mol Yb})^{-1}$, a value $\mathcal{R}_W = 0.8$ is obtained and is typical of intermediate valence and heavy fermion systems.

3.4. Electrical resistivity

Shown in figure 3 is the electrical resistivity $\rho(T)$ of $Yb_3Ni_5Al_{19}$. Metallic behaviour is observed in this material with the presence of a small shoulder at ~100 K, characteristic of

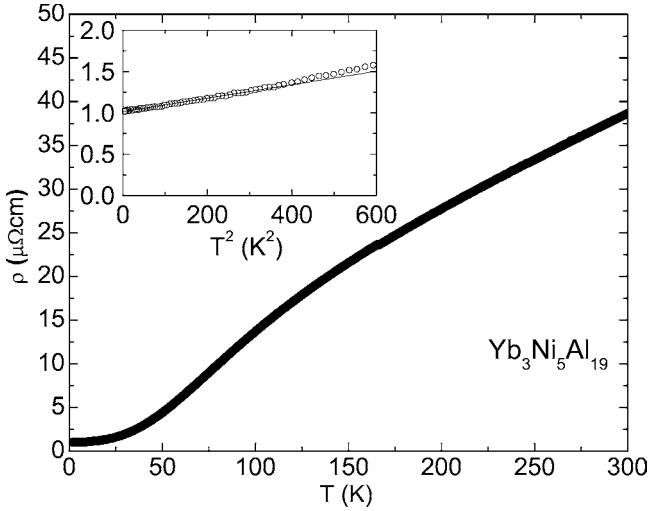

Figure 3. The electrical resistivity $\rho(T)$ of $Yb_3Ni_5Al_{19}$. Inset: $\rho(T)$ versus T^2. The solid line is a linear fit of the data.

intermediate valence systems. The residual resistivity ratio RRR $\equiv \rho(300\ \mathrm{K})/\rho(2\ \mathrm{K}) \simeq 40$ indicates the high quality of the single crystals. The resistivity exhibits a Fermi liquid temperature dependence, i.e., $\rho = \rho_0 + AT^2$, as shown in the inset of figure 3. A linear fit of the data for $2\ \mathrm{K} \leqslant T \leqslant 17\ \mathrm{K}$ yields $\rho_0 = 1.0\ \mu\Omega$ cm and $A = 0.8 \times 10^{-4}\ \mu\Omega$ cm K^{-2}. From this value of A, an estimate of the electronic specific heat coefficient $\gamma \sim 45$ mJ K^{-2} (mol Yb)$^{-1}$ is obtained using the empirical relation $A/\gamma^2 = 4 \times 10^{-7}\ \mu\Omega$ cm (mol Yb)^2 K^2 mJ^{-2} appropriate for Yb-based intermediate valence systems [12], in reasonable agreement with the thermodynamic properties described above.

4. Discussion

For many Yb-based intermediate valence systems, the single-impurity calculations of Rajan [13] based on the Coqblin–Schrieffer model quantitatively describe the measured magnetic susceptibility. However, in many Kondo lattice compounds, which often have strong intersite coupling and where CEF effects may play an important role, a more sophisticated theory is needed. To address this issue, calculations were performed using the Anderson impurity model for valence fluctuations between one magnetic configuration and one non-magnetic configuration including crystal electric field effects; in addition, the interactions between the Yb ions were taken into account using a mean field approximation. The impurity is treated in an approximation scheme developed in [14, 15] based on the non-crossing approximation (NCA), generalized to allow for different hybridizations of each crystal field multiplet of the magnetic configuration with the band. The details are given in [2]. In [2, 14, 15], the density of states of the non-magnetic configuration $\rho_0(\omega)$ is replaced by its pole at temperature $T = 0$, and the ground state energy is obtained by a variational ansatz which is exact for large degeneracy of the magnetic configuration [16]. This approximation ceases to be valid at temperatures of the order of the charge transfer energy and, at high temperatures, the result lies below that of the full NCA treatment. In spite of this shortcoming, this additional approximation has led to very good agreement with results for the magnetic susceptibility of the full NCA and Bethe ansatz in the isotropic case [15]. Furthermore, it has the advantage that the results converge smoothly to those of the variational approximation for $T = 0$ and

is free from the usual artifacts of the NCA at low T [17]. To reduce the number of free parameters in the fit, we assume an axial crystal field, as in [14, 15]. Also, the large ratio of the value of the magnetic susceptibility at its maximum over its value at zero temperature points to a large effective degeneracy [13]. Therefore, we assume no splitting of the ground state multiplet and took only two different hybridizations of the doublets with the conduction band, one for the low angular momentum projection ($m = \pm 1/2, 3/2$) and another for the high projection ($m = \pm 5/2, 7/2$). The susceptibility is calculated as an average $\chi = (2\chi_\perp + \chi_\parallel)/3$, where $\chi_\parallel$ ($\chi_\perp$) is the susceptibility for the magnetic field parallel (perpendicular) to the main axis. For each direction α, the susceptibility in the compound χ_α is related to the impurity one χ^0_α by the mean field expression $\chi_\alpha = \chi^0_\alpha/(1 + I\chi^0_\alpha)$, where I includes the effects of the exchange interactions of all sites that interact with a given one. The free parameters are I, the f occupation number of Yb at $T = 0$, n_f, and the two $\Gamma_m = \pi\rho_c V_m^2$, where ρ_c is the density of states of the conduction band (assumed constant) and V_m is the hybridization of each of the doublets with the conduction band.

Figure 2 shows a comparison of the data and the two impurity model calculations of Rajan [13] (with $T_K = 435$ K and $\chi_0 = 2.28 \times 10^{-3}$ cm^3/mol Yb as input parameters) and the NCA discussed above. The NCA fit was obtained taking all CEF doublets at the same energy, $\Gamma_m = 90$ K for $m = \pm 1/2$ and $3/2$, and $\Gamma_m = 50$ K for $m = \pm 7/2$ and $5/2$, from which a Kondo temperature $T_K = 436$ K is deduced. A significant degree of intermediate valence is also predicted: $n_f = 0.45$ (valence $\nu = 2 + n_f = 2.45$). A large value $I = 250$ mol Yb cm^{-3} also stresses the importance of strong antiferromagnetic correlations in $Yb_3Ni_5Al_{19}$. The discrepancy between data and the theoretical curve for $T > 250$ K is probably a consequence of the additional approximation for $\rho_0(\omega)$ mentioned above and can be improved if the full NCA treatment is used. Despite these shortcomings, the agreement between the data and the NCA calculations is reasonable; furthermore, with the inclusion of CEF effects and intersite interactions, the NCA calculations provide a better model of the magnetic susceptibility of $Yb_3Ni_5Al_{19}$ than the calculations based on the Coqblin–Schrieffer model [13] (figure 2).

The specific heat can be estimated from the density of states obtained using the above mentioned variational ansatz [16] which yields $\gamma = 62$ mJ K^{-2} (mol Yb)$^{-1}$, a factor of two larger than the experimental result. The calculated γ does not include a quasiparticle renormalization constant or the effect of interatomic interactions. Closer agreement between the calculated and experimental γ is expected if intersite interactions are included which move entropy to higher temperatures, thereby reducing the low T specific heat. It should be mentioned that the specific heat coefficient determined from the Coqblin–Schrieffer model [13] is $\gamma = 160$ mJ K^{-2} (mol Yb)$^{-1}$ using $T_K = 435$ K obtained from a fit to the $\chi(T)$ data (figure 2), a factor of 5 larger than the experimental value.

The compound $Yb_3Ni_5Al_{19}$ belongs to a growing number of Yb–Ni–Al systems which exhibit strongly correlated electron behaviour. YbNiAl displays both antiferromagnetic order at $T_N = 3$ K and heavy fermion characteristics with $\gamma \sim 350$ mJ mol^{-1} K^{-2} [18]. The $YbNiAl_2$ system also apparently orders magnetically [19]. Non-Fermi liquid behaviour is observed in Yb_2Ni_2Al in which $C/T \sim -\ln T$ below 4 K and reaches a value $\gamma \sim 700$ mJ mol^{-1} K^{-2} at $T = 0.5$ K suggesting that this material is close to a quantum critical point [20]. The application of pressure of 85 kbar induces magnetic order at $T_m \sim 1.8$ K in this material [21], as expected from a decrease of $\mathcal{J}$ with pressure often observed in Yb intermetallic systems [1]. It appears that the hybridization between the f electrons and conduction electrons is stronger (larger $\mathcal{J}$) in $Yb_3Ni_5Al_{19}$, which has a number of short Yb–Al bonds, giving rise to intermediate valence behaviour, similar to that of $YbAl_3$ [22]. It would be of interest to investigate the Ce–Ni–Al and U–Ni–Al phase diagrams to search for isostructural compounds that also display strongly correlated electron behaviour.

5. Conclusions

Single crystals of $Yb_3Ni_5Al_{19}$ have been characterized by means of magnetic susceptibility, specific heat, and electrical resistivity measurements. The physical properties indicate that $Yb_3Ni_5Al_{19}$ is an intermediate valence compound with a characteristic energy scale $T_K \sim 500$ K. Calculations of $\chi(T)$ based on the Anderson impurity model within the NCA including CEF effects suggest a large deviation from trivalent behaviour ($n_f = 0.45$) and stress the importance of strong antiferromagnetic correlations in this material.

Acknowledgments

We would like to thank C D Batista for useful discussions. The work at Los Alamos was performed under the auspices of the DOE. The work in Argentina was sponsored by PICT 03-12742 of ANPCyT. Two of us (AL, AAA) are partially supported by CONICET. SB is partially supported by an ICAM fellowship.

References

[1] Thompson J D and Lawrence J M 1994 *Handbook on the Physics and Chemistry of the Rare Earths* vol 19, ed K A Gschneidner Jr, L Eyring, G H Lander and G R Choppin (Amsterdam: North-Holland) chapter 133, p 383
[2] Moreno N O 2004 unpublished
[3] Grin Y and Rogl P 1989 *Inorg. Mater.* **25** 514
[4] Buschinger B, Geibel C, Weiden M, Dietrich C, Cordier G, Olesch G, Köhler J and Steglich F 1997 *J. Alloys Compounds* **260** 44
[5] Buschinger B, Trovarelli O, Weiden M, Geibel C and Steglich F 1998 *J. Alloys Compounds* **275–277** 633
[6] Trovarelli O, Geibel C, Buschinger B, Borth R, Mederle S, Grosche M, Sparn G, Steglich F, Brosch O and Donnevert L 1999 *Phys. Rev.* B **60** 1136
[7] Dhar S K, Mitra C, Bonville P, Rams M, Królas K, Godart C, Alleno E, Suzuki N, Miyake K, Watanabe N, Onuki Y, Manfrinetti P and Palenoza A 2001 *Phys. Rev.* B **64** 094423
[8] Gladshevskii R E, Cenzual K and Parthé E 1992 *J. Solid State Chem.* **100** 9
[9] Rykhal R M, Zarechnyuk O S and Yarmolyuk Y P 1972 *Sov. Phys.—Crystallogr.* **17** 453
[10] Gladshevskii R E and Parthé E 1992 *Z. Kristallogr.* **198** 171
[11] Aldred A T 1975 *Phys. Rev.* B **11** 2597
[12] Tsujii N, Yoshimura K and Kosuge K 2003 *J. Phys.: Condens. Matter* **15** 1993
[13] Rajan V T 1983 *Phys. Rev. Lett.* **51** 308
[14] Zevin V, Zwicknagl G and Fulde P 1988 *Phys. Rev. Lett.* **60** 2331
[15] Zwicknagl G, Zevin V and Fulde P 1990 *Z. Phys.* B **79** 365
[16] Gunnarsson O and Schönhammer K 1983 *Phys. Rev.* B **28** 4315
[17] Müller-Hartmann E 1984 *Z. Phys.* B **57** 281
[18] Schank C, Olesch G, Koöler J, Tegel U, Diehl U K J, Klimm S, Sparn G, Horn S, Geibel C and Steglich F 1995 *J. Magn. Magn. Mater.* **140–144** 1237
[19] Geibel C, Klinger U, Buschinger B, Weiden M, Olesch G, Thomas F and Steglich F 1996 *Physica* B **223/224** 370
[20] Stewart G R 2001 *Rev. Mod. Phys.* **73** 797
[21] Winkelmann H, Abd-Elmeguid M M, Micklitz H, Sanchez J P, Geibel C and Steglich F 1998 *Phys. Rev. Lett.* **81** 4947
[22] Klaasse J C P, Mattens W C M, de Boer F R and de Chatel P F 1977 *Physica* B **86–88** 234